



Predicting pathological subtypes and stages of thymic epithelial tumors using DWI: value of combining ADC and texture parameters

Bo Li¹ · Yong-kang Xin¹ · Gang Xiao¹ · Gang-feng Li¹ · Shi-jun Duan¹ · Yu Han¹ · Xiu-long Feng¹ · Wei-qiang Yan¹ · Wei-cheng Rong¹ · Shu-mei Wang² · Yu-chuan Hu¹ · Guang-bin Cui¹

Received: 3 September 2018 / Revised: 16 January 2019 / Accepted: 7 February 2019 / Published online: 15 March 2019
© European Society of Radiology 2019

Abstract

Objectives To explore the value of combining apparent diffusion coefficients (ADC) and texture parameters from diffusion-weighted imaging (DWI) in predicting the pathological subtypes and stages of thymic epithelial tumors (TETs).

Methods Fifty-seven patients with TETs confirmed by pathological analysis were retrospectively enrolled. ADC values and optimal texture feature parameters were compared for differences among low-risk thymoma (LRT), high-risk thymoma (HRT), and thymic carcinoma (TC) by one-way ANOVA, and between early and advanced stages of TETs were tested using the independent samples *t* test. Receiver operating characteristic (ROC) curve analysis was performed to determine the differentiating efficacy.

Results The ADC values in LRT and HRT were significantly higher than the values in TC ($p = 0.004$ and 0.001 , respectively), also in early stage, values were significantly higher than ones in advanced stage of TETs ($p < 0.001$). Among all texture parameters analyzed in order to differentiate LRT from HRT and TC, the V_{312} achieved higher diagnostic efficacy with an AUC of 0.875, and combination of ADC and V_{312} achieved the highest diagnostic efficacy with an AUC of 0.933, for differentiating the LRT from HRT and TC. Furthermore, combination of ADC and V_{1030} achieved a relatively high differentiating ability with an AUC of 0.772, for differentiating early from advanced stages of TETs.

Conclusions Combination of ADC and DWI texture parameters improved the differentiating ability of TET grades, which could potentially be useful in clinical practice regarding the TET evaluation before treatment.

Key Points

- DWI texture analysis is useful in differentiating TET subtypes and stages.
- Combination of ADC and DWI texture parameters may improve the differentiating ability of TET grades.
- DWI texture analysis could potentially be useful in clinical practice regarding the TET evaluation before treatment.

Keywords Thymic epithelial tumors · Neoplasm staging · Diffusion magnetic resonance imaging · Texture analysis

Bo Li and Yong-kang Xin contributed equally to this work.

Electronic supplementary material The online version of this article (<https://doi.org/10.1007/s00330-019-06080-4>) contains supplementary material, which is available to authorized users.

✉ Yu-chuan Hu
hyc3140@126.com

✉ Guang-bin Cui
cgibt@126.com; cuigbt@fmmu.edu.cn

¹ Department of Radiology and Functional and Molecular Imaging Key Lab of Shaanxi Province, Tangdu Hospital, Military Medical University of PLA Airforce (Fourth Military Medical University), Xi'an 710038, Shaanxi, People's Republic of China

² Department of Pathology, Tangdu Hospital, Military Medical University of PLA Airforce (Fourth Military Medical University), Xi'an 710038, Shaanxi, People's Republic of China

Abbreviations

ADC	Apparent diffusion coefficient
CT	Computed tomography
DWI	Diffusion-weighted imaging
FOV	Field of view
HRT	High-risk thymoma
LRT	Low-risk thymoma
MRI	Magnetic resonance imaging
NEX	Number of excitations
ROC	Receiver operating characteristic
ROI	Region of interest
TC	Thymic carcinoma
TE	Echo time
TETs	Thymic epithelial tumors
TR	Repetition time

VOI Volume of interest
WHO World Health Organization

Introduction

Thymic epithelial tumors (TETs) are relatively rare tumors, accounting for 0.2–1.5% of adult malignancies, but they represent the most common primary tumors of the anterior mediastinum [1, 2]. Masaoka staging and World Health Organization (WHO) pathological classification are the major prognostic indicators in addition to resectability [3, 4]. Clinical management of TETs is mainly dependent on the pathological subtypes and stages [5]. Early-stage (stages I and II) TETs are generally treated with surgery, and advanced stage (stages III and IV) of TETs frequently recommend a multimodality treatment regime [5–9]. Therefore, it is critically important to accurately identify the risk grades of TETs before treatment for guiding treatment decision-making.

Imaging diagnosis and risk grades of TETs would be valuable and desirable for determining appropriate treatment strategies [10]. Computed tomography (CT) and conventional magnetic resonance imaging (MRI) are used as routine imaging modalities for TET patients, and they can provide detailed morphologic information regarding tumor location, shape, contour, homogeneity, infiltration, and so on [11–14]. Although conventional imaging showed considerable potential, these examination methods depend on qualitative parameters, with many degrees of overlap among different entities, and cannot quantitatively assess the subtypes and stages of TETs accurately [4].

With the technical advances in fast MR imaging, diffusion-weighted imaging (DWI) has been successfully used in studies of lung cancer, mediastinal tumors, and pleural lesions [15–17]. DWI is considered the most sensitive method to detect the differences of water molecular diffusion in living tissues [18], and the apparent diffusion coefficient (ADC) value obtained by using a monoexponential model, providing information on tumor cellularity, can be potentially useful in quantitatively differentiating the grades of TETs [9, 19, 20].

Texture analysis evaluates the distribution of signal intensity at a pixel level within a tumor to quantify the tumor heterogeneity, which occurs due to variations in genomic subtypes, cell proliferation or apoptosis, metabolic activity, vascular structure, and other factors [21]. Comparing with morphological analysis of conventional imaging, texture parameters provide a more detailed and quantitative information on tumor composition through a pixel-by-pixel analysis. A series of texture analysis studies have demonstrated a potential role in differential diagnosis, staging, and predicting prognosis on different tumors [22–27]. However, it remains largely

unknown whether DWI texture analysis can improve the efficacy in predicting the grades of TETs.

In the present study, we aimed to evaluate the potential value of combining ADC and DWI texture parameters in predicting the pathological subtypes and stages of TETs preoperatively.

Materials and methods

Subjects

This retrospective single-center study was approved by the local Ethics Committee, and informed consent was waived.

Between December 2013 and March 2016, 91 consecutive patients with suspected TETs based on CT underwent conventional MRI and DWI examination of the thorax, and the final diagnosis was based on pathological analysis. Of these, 20 patients were excluded for non-TETs diagnosis based on pathological evaluation, 11 patients were excluded for poor image quality or motion artifact, and 3 patients were excluded for solid part of the tumor <2.0 cm in size. The final study population was comprised of 57 patients (36 men, 21 women; mean age, 48.9 ± 11.4 years) with newly diagnosed TETs according to the pathological results (Fig. 1 and Table 1).

Thorax MRI protocol

All patients were examined preoperatively with the same imaging acquisition protocol on a 3.0-T whole-body system (MR750, GE Healthcare) with a 40-mT/m maximum gradient capability and a standard 8-channel torso coil. Conventional MRI and DWI were performed in regular

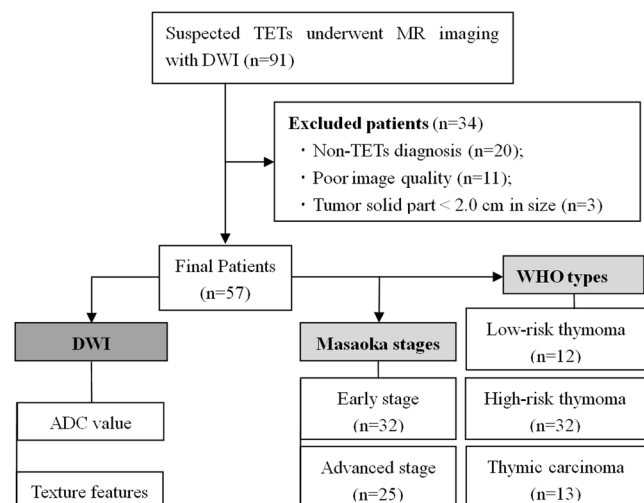


Fig. 1 Flow diagram of patient selection, quantitative metrics, and grouping

Table 1 Clinical and demographic characteristics of 57 patients with thymic epithelial tumor

Patient characteristics	
Age (years)	
Mean \pm SD	48.9 \pm 11.4
Sex—no. (%)	
Males	36 (63.2)
Females	21 (36.8)
Major symptoms or signs—no. (%)	
No symptom	10 (17.5)
Myasthenia gravis	15 (26.3)
Chest pain	14 (24.6)
Respiratory symptoms	11 (19.3)
Other	7 (12.3)
Method for obtaining pathologic results—no. (%)	
Surgery	47 (82.5)
Puncture biopsy	10 (17.5)
Masaoka–Koga stage—no. (%)	
Stage I	17 (29.8)
Stage II	15 (26.3)
Stage III	7 (12.3)
Stage IV	18 (31.6)
WHO classification—no. (%)	
Thymoma	44(77.3)
A	1 (1.8)
AB	8 (14.0)
B1	3 (5.3)
B2	23 (40.4)
B3	9 (15.8)
Thymic carcinoma	13 (22.7)
Squamous cell carcinoma	7 (12.3)
Adenocarcinoma	3 (5.2)
Neuroendocrine carcinomas	3 (5.2)

sequence during the same examination. The conventional MRI protocol included respiratory triggering T1-weighted spin-echo in the axial plane, T2-weighted fast spin-echo in the axial planes and coronal planes, and axial T2-weighted turbo spin-echo images with fat suppression. Subsequently, DWI sequences ($b = 1000 \text{ s/mm}^2$) were performed with a single-shot diffusion-weighted spin-echo echo-planar sequence. We used the respiratory triggering and chemical shift-selective fat suppression technique to reduce the artifacts. Parallel imaging was used with an acceleration factor of 2. A local shim box covering the whole thorax was applied to minimize the susceptibility artifacts. Other parameters were as follows: TR/TE, 6000 ms/51 ms; matrix size, 96×128 ; FOV, $40 \text{ cm} \times 40 \text{ cm}$; slice thickness, 5 mm; gap, 0.5 mm; NEX, 4. The total scan time was approximately 1 min and 33 s.

ADC value measurement

All data were analyzed on a GE ADW4.6 workstation. The mean ADC values were measured independently by one experienced radiologist (B.L., with 15 years of experience in MRI) using a commercial software (Functool 9.4.05, GE Healthcare). He was aware that the patients had TETs, but blinded to the pathological subtypes of the tumors. First, he reviewed the conventional MR images carefully to determine the solid part of each tumor. Next, the DWI data were analyzed. Two circular regions of interest (ROIs) were manually drawn using an electronic cursor in the slice containing the largest cross-sectional area, which were placed to include the solid tumor elements by defining ROIs based on the relatively high signal intensity on the DW image (bright region, $b = 1000 \text{ s/mm}^2$, as shown in Fig. 2a) or the relatively low ADC value in the ADC map (deep-blue region, as shown in Fig. 2b), avoiding large vessels and hemorrhagic, cystic, and necrotic areas. The mean ROI area was $46.9 \pm 20.2 \text{ mm}^2$ (range, $11.5\text{--}88.0 \text{ mm}^2$). The ADC value was calculated by fitting the b_0 image and DW images at $1000 \text{ s/mm}^2 b$ value into the conventional ADC equation (Eq. (1)) [28]:

$$S_b/S_0 = \exp(-b \text{ ADC}) \quad (1)$$

The ADC maps were generated automatically (as shown in Fig. 2b) and the mean ADC values within two ROIs were obtained. The final ADC is the average of the ADC values of two ROIs.

DWI texture analysis

Tumor segmentation

All images were anonymized and stored in DICOM format. One experienced radiologist (B.L., with 15 years of experience in MRI) manually segmented the tumor area on axial DW images by using commercial software applications, NordiICE (Version 4.0.4, NordicNeuroLab). A volume of interest (VOI) was drawn manually around the entire cross-sectional tumoral region in three consecutive slices containing the largest cross-sectional area on DW images in a slice-by-slice method. Care was taken to exclude adjacent tissues, attempting to maintain an approximate distance of 1–2 mm away from the tumor margin to minimize the partial volume phenomenon (Fig. 2c).

Feature extraction

Using a non-commercial Analysis-Kit software (GE Healthcare), the quantitative features were extracted on DW images based on the drawn VOI in the previous step. Forty-

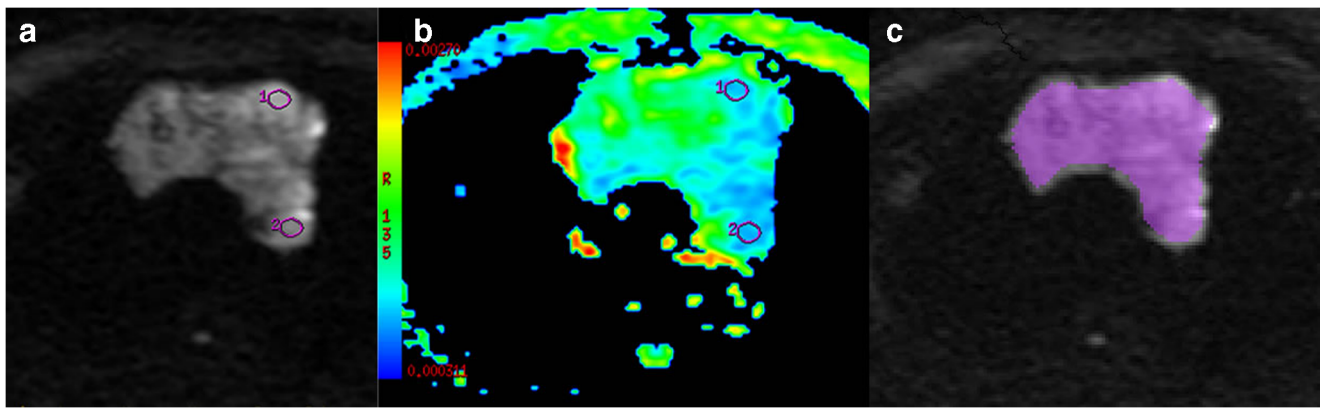


Fig. 2 The schematic diagram of tumor segmentation. Two circular regions of interest were drawn to include the solid tumor elements by defining ROIs based on the relatively high signal intensity on the DW image (a, bright region, $b = 1000 \text{ s/mm}^2$), or the relatively low ADC

value in the ADC map (b, deep-blue region), and a volume of interest (VOI) was drawn around the entire cross-sectional tumor region in three consecutive slices on DW images (c)

two first-order histograms, 983 second-order textures (432 gray-level co-occurrence matrix, 540 gray-level run length matrix, and 11 gray-level size zone matrix), 9 form factors, and 10 Haralick features were extracted; thus, a total of 1044 quantitative features were obtained from the original images. Detail descriptions regarding the quantitative features extracted in this study are presented in *Supplemental file (Texture parameters description.docx)*.

Feature selection

Due to the large number of features, we applied a three-step feature selection process to remove irrelevant or redundant features and identify ones that are the most informative. First, one-way ANOVA was used to test for significant differences of texture features among low-risk thymoma (LRT), high-risk thymoma (HRT), and thymic carcinoma (TC) groups, and features with p value < 0.01 were kept for further feature selection. Similarly, independent samples t test was used to test for significant differences of texture features between early and advanced TETs, and $p < 0.05$ as the selecting criteria. Further reduction of features was conducted by Pearson's correlation tests. When the Pearson correlation coefficient of any two features was larger than 0.9, one of them was selected at random, and the rest could be treated in the same manner [29]. Finally, the optimal feature with the best discriminative performance from similar category was selected.

Pathologic diagnosis

The final diagnosis was determined by surgical or puncture biopsy specimen and confirmed with pathologic analysis, which was performed by an expert in the pathology department, who was blinded to the MR findings. Based on the criteria of the 2004 World Health Organization (WHO)

histological classification and Jeong simplification classification of the thymic tumors [30, 31], TETs were divided into three subgroups: LRT (types A, AB, and B1), HRT (types B2 and B3), and TC. Early (stages I and II) and advanced stages (stages III and IV) of TETs were defined according to the Masaoka staging system [3].

Statistical analysis

The Kolmogorov–Smirnov (K–S) test was used to assess the normality of data distributions. Numerical variables with normal distribution were denoted as mean and standard deviation. The ADC value and DWI texture parameters in TETs were compared for differences among LRT, HRT, and TC groups with one-way ANOVA (equal variances assumed) or Brown–Forsythe test (equal variances not assumed), and further post hoc multiple comparisons were performed with Bonferroni test (equal variances assumed) or Dunnett's T3 test (equal variances not assumed). The ADC value and texture parameters between early (Masaoka stages I and II) and advanced (stages III and IV) stages of TETs were tested for differences using the independent samples t test. The binary logistic regression analysis was used in evaluating the effects of combination of multiple parameters. Receiver operating characteristic (ROC) curve analyses were performed to determine optimum thresholds for differentiating the defined groups by various parameters, and also to calculate the sensitivity, specificity, and area under the curve (AUC). The leave one out cross-validation (LOOCV) was used in resampling in the area under the ROC curve. All statistical analyses above were performed with IBM SPSS 20.0 software (IBM Corp). Differences between the AUCs were compared by using a Delong test and performed using Medcalc version 18.5 software (MedCalc). Statistical significance was accepted as $p < 0.05$.

Results

Demographic characteristics

Table 1 exhibits the demographic characteristics of the patients. The major clinical features of the patients include myasthenia gravis (26.3%; 15 of 57 patients), chest pain (24.6%; 14 of 57), respiratory symptoms (19.3%; 11 of 57), and others (12.3%; 7 of 57), and no symptom in 10 patients (17.5%).

Forty-seven TET patients were staged based on surgical specimen, and the other 10 advanced-stage patients who were proved by puncture biopsy were staged by the presence of pleural or pericardium implants or metastasis at imaging. According to the Masaoka stages, 17 (29.8%) patients were in clinical stage I, 15 (26.3%) in clinical stage II, 7 (12.3%) in stage III, and 18 (31.6%) in stage IV. As for the pathological subtypes, 12 patients had LRT (types A ($n = 1$), AB ($n = 8$), and B1 ($n = 3$)); 32 HRT (types B2 ($n = 23$) and B3 ($n = 9$)); and 13 TC (squamous cell carcinoma ($n = 7$), adenocarcinoma ($n = 3$), and neuroendocrine carcinomas ($n = 3$)). The relationship between Masaoka stage and the simplified WHO histologic classification is shown in Table 2. None of LRTs was in the advanced stage (stages III and IV) compared with 12 of 32 (37.5%) HRTs, and all of 13 TC patients.

Comparison of ADC values and DWI texture parameters among low-risk thymomas, high-risk thymomas, and thymic carcinomas

After feature selection, seven texture parameters with good discriminative performance were obtained, including V_{80} (*Cluster Shade_angle90_offset1*), V_{140} (*GLCM Entropy_AllDirection_offset3*), V_{153} (*Cluster Prominence_AllDirection_offset3_SD*), V_{204} (*GLCM Entropy_angle0_offset4*), V_{296} (*Cluster Shade_AllDirection_offset6_SD*), V_{312} (*Cluster Shade_angle45_offset6*), and V_{735} (*Short Run Emphasis_AllDirection_offset5_SD*). The statistic results of the ADC and selected texture parameters among LRTs, HRTs, and TCs are shown in Table 3 and Fig. 3.

Table 2 Relationship between histopathological subtypes and Masaoka stages of thymic epithelial tumors

	LRT ($n = 12$)	HRT ($n = 32$)	TC ($n = 13$)	Total
Stage I	9 (75.0%)	8 (25.0%)	0	17 (29.8%)
Stage II	3 (25.0%)	12 (37.5%)	0	15 (26.3%)
Stage III	0	3 (9.4%)	4 (30.8%)	7 (12.3%)
Stage IV	0	9 (28.1%)	9 (69.2%)	18 (31.6%)

LRT, low-risk thymoma; HRT, high-risk thymoma; TC, thymic carcinoma

The mean ADC values in LRTs or HRTs were significantly higher than ones in TC groups according to the one-way ANOVA (ADC, 1.63, 1.30, and $0.86 \times 10^{-3} \text{ mm}^2/\text{s}$, $p = 0.004$ and 0.001 , respectively), while there were no significant differences in ADC values between the LRT and HRT groups ($p > 0.017$). With regard to 7 selected DWI texture features, significant differences were found among LRT, HRT, and TC groups (all $p < 0.05$). After further post hoc multiple comparisons, V_{80} and V_{312} values in LRTs were significantly higher than ones in HRT or TC groups (all $p < 0.017$).

Comparison of ADC values and DWI texture parameters between early and advanced stages of TETs

After feature selection, nine texture parameters with better discriminative performance remained, including V_{57} (*Cluster Prominence_AllDirection_offset1_SD*), V_{204} (*GLCM Entropy_angle0_offset4*), V_{278} (*Correlation_angle135_offset5*), V_{296} (*Cluster Shade_AllDirection_offset6_SD*), V_{735} (*Short Run Emphasis_AllDirection_offset5_SD*), V_{920} (*High Gray-Level Run Emphasis_AllDirection_offset8_SD*), V_{1025} (*Sphericity*), V_{1030} (*Maximum 3D Diameter*), and V_{1033} (*Spherical Disproportion*). The statistic results of the ADC and selected texture parameters between early and advanced TETs are shown in Table 4 and Fig. 4.

The mean ADC value in early-stage TETs was significantly higher than that in advanced-stage TETs (1.48 vs. $1.00 \times 10^{-3} \text{ mm}^2/\text{s}$, $p < 0.001$). As for the nine selected DWI texture parameters, significant differences were found between early and advanced stages of TETs (all $p < 0.05$).

ROC analysis

Based on the ROC analyses, the V_{80} and V_{312} values achieved higher diagnostic efficacy with an AUC of 0.862 and 0.875, the same sensitivity of 75.0%, and specificity of 88.1% and 90.5%, for differentiating the LRT from HRT and TC at the cutoff value of 1.29×10^6 and 5.00×10^5 , respectively. As for the ADC value, the AUC, sensitivity, specificity, and the cutoff value for differentiating the LRT from HRT or TC were 0.746, 50.0%, 90.5%, and $1.86 \times 10^{-3} \text{ mm}^2/\text{s}$, respectively. In addition, we made a binary logistic regression by using the group as a dependent variable and using V_{80} and V_{312} or ADC and V_{312} as covariates, and then acquired each patient's predicted probability (p value). These p values were then analyzed by ROC curve analysis. Logistic (ADC, V_{312}) achieved the highest diagnostic efficacy with an AUC of 0.933, sensitivity of 95.2%, and specificity of 91.7%, and logistic (V_{80} , V_{312}) did not improved the differentiating efficacy with an AUC of 0.877 (Table 5 and Fig. 5a). Pairwise comparison of the AUCs revealed that AUC of logistic (ADC, V_{312}) was

Table 3 ADC and DWI texture parameter comparisons among low-risk thymoma, high-risk thymoma, and thymic carcinoma

Parameters	LRT (<i>n</i> = 12)	HRT (<i>n</i> = 32)	TC (<i>n</i> = 13)	<i>p</i>
ADC ($\times 10^{-3}$ mm ² /s)	1.63 \pm 0.63	1.30 \pm 0.51	0.86 \pm 0.20 ^{#§}	0.002*
Texture analysis				
V ₈₀ ($\times 10^6$)	1.57 \pm 0.68	0.75 \pm 0.70 [#]	0.67 \pm 0.54 [#]	0.001
V ₁₄₀	9.02 \pm 1.02	9.93 \pm 1.14	10.47 \pm 1.02 [#]	0.006
V ₁₅₃ ($\times 10^7$)	7.46 \pm 5.77	3.67 \pm 3.03	2.46 \pm 1.75	0.016*
V ₂₀₄	8.96 \pm 1.12	9.79 \pm 1.27	10.48 \pm 1.02 [#]	0.009
V ₂₉₆ ($\times 10^5$)	3.00 \pm 2.03	1.52 \pm 1.41	0.82 \pm 0.53 [#]	0.005*
V ₃₁₂ ($\times 10^5$)	8.24 \pm 5.60	1.44 \pm 2.14 [#]	2.14 \pm 3.56 [#]	< 0.001*
V ₇₃₅ ($\times 10^{-3}$)	7.14 \pm 3.97	4.01 \pm 2.30 [#]	4.33 \pm 3.04	0.008

* *p* values were calculated by Brown–Forsythe *F* test (unequal variances), and the other *p* values were obtained based on one-way ANOVA (equal variances). [#] Significant difference compared with LRT group. [§] Significant difference compared with the HRT group based on post hoc multiple comparisons (*p* < 0.017)

LRT, low-risk thymoma; HRT, high-risk thymoma; TC, thymic carcinoma; ADC, apparent diffusion coefficients; V₈₀, Cluster Shade_angle90_offset1; V₁₄₀, GLCM Entropy_AllDirection_offset3; V₁₅₃, Cluster Prominence_AllDirection_offset3_SD; V₂₀₄, GLCM Entropy_angle0_offset4; V₂₉₆, Cluster Shade_AllDirection_offset6_SD; V₃₁₂, Cluster Shade_angle45_offset6; V₇₃₅, Short Run Emphasis_AllDirection_offset5_SD

significantly higher than AUC of ADC value for differentiating the LRT from HRT and TC (*p* = 0.0147), but no significant differences were found between AUCs from any other parameters (all *p* > 0.05).

As shown in Table 5 and Fig. 5b, for differentiating early from advanced stages of TETs, the ADC value obtained a relatively high differentiating ability with an AUC of 0.755, sensitivity of 68.8%, and specificity of 76.0% at the cutoff value of 1.18×10^{-3} mm²/s. The AUC, sensitivity, and specificity for V₂₀₄, V₁₀₃₀, and logistic (ADC, V₁₀₃₀), respectively, were as follows: V₂₀₄, 0.720, 68.0%, and 75.0%; V₁₀₃₀, 0.726, 92.0%, and 56.3%; and logistic (ADC, V₁₀₃₀), 0.772, 84.0%, and 65.6%. Pairwise comparison of the AUCs revealed no significant differences between AUCs from the above parameters for differentiating early from advanced stages of TETs (all *p* > 0.05).

In the discriminant analysis performed across the two subtypes (LRT vs. HRT and TC), 92.6% of original or cross-validated grouped cases were correctly classified by ADC+V₃₁₂, and 71.9% of original or cross-validated grouped cases were correctly classified across the two stages (early vs. advanced stages) by ADC+V₁₀₃₀ according to the LOOCV procedure.

Discussion

As a crucial big-data source for the mining of large information, digital medical images are routinely acquired for almost every patient with tumor, and texture analysis is rapidly becoming a noninvasive means of lesion characterization and classification for improved decision support [32]. In this study, we evaluated whether the DWI texture analysis could be used to predict the histological subtypes

and stages of TETs. The results revealed significant differences of several texture parameters in different pathological subtypes or stages of TETs, and combination of ADC and V₃₁₂ significantly improved the differentiating ability of subtypes than ADC alone, which could potentially be used in clinical practice regarding the TET evaluation before treatment.

Stage and histological type were two of the most important factors that bridge the biology and clinical behavior of TETs [33]. WHO histological subtypes of TETs were correlated with clinical stages [19, 34]. Accurate identification of TET risk grades before treatment is a crucial question facing clinicians and radiologists for guiding therapeutic strategies. In this study, all of the LRTs were early stage, and most of HRTs and all TCs were advanced disease. Therefore, to a certain extent, pathological classification was correlated with the clinical stage of TETs.

Previous studies showed that the ADC value was helpful in differentiating different subtypes or stages of TETs [9, 19, 20]. Similarly, our results also found different mean ADC values among different subtypes or stages of TETs. Comparing with the LRT or early-stage TETs, the HRT and TC or advanced-stage TETs have more significantly enlarged nuclei and show hypercellularity, consequently leading to the decreased ADC value [19, 20].

The various parameters derived from imaging texture analysis are biologically regarded as good indices of tumor heterogeneity, which were thought to result from regional differences in tumor cellularity, proliferation, angiogenesis, hypoxia, and necrosis, all of which are related to tumor risk grades [35, 36]. Two recent studies differentiated the pathological subtypes of TETs using PET/CT textural features and demonstrated its potential value in TET tumor grades [27, 35]. In this study, the results

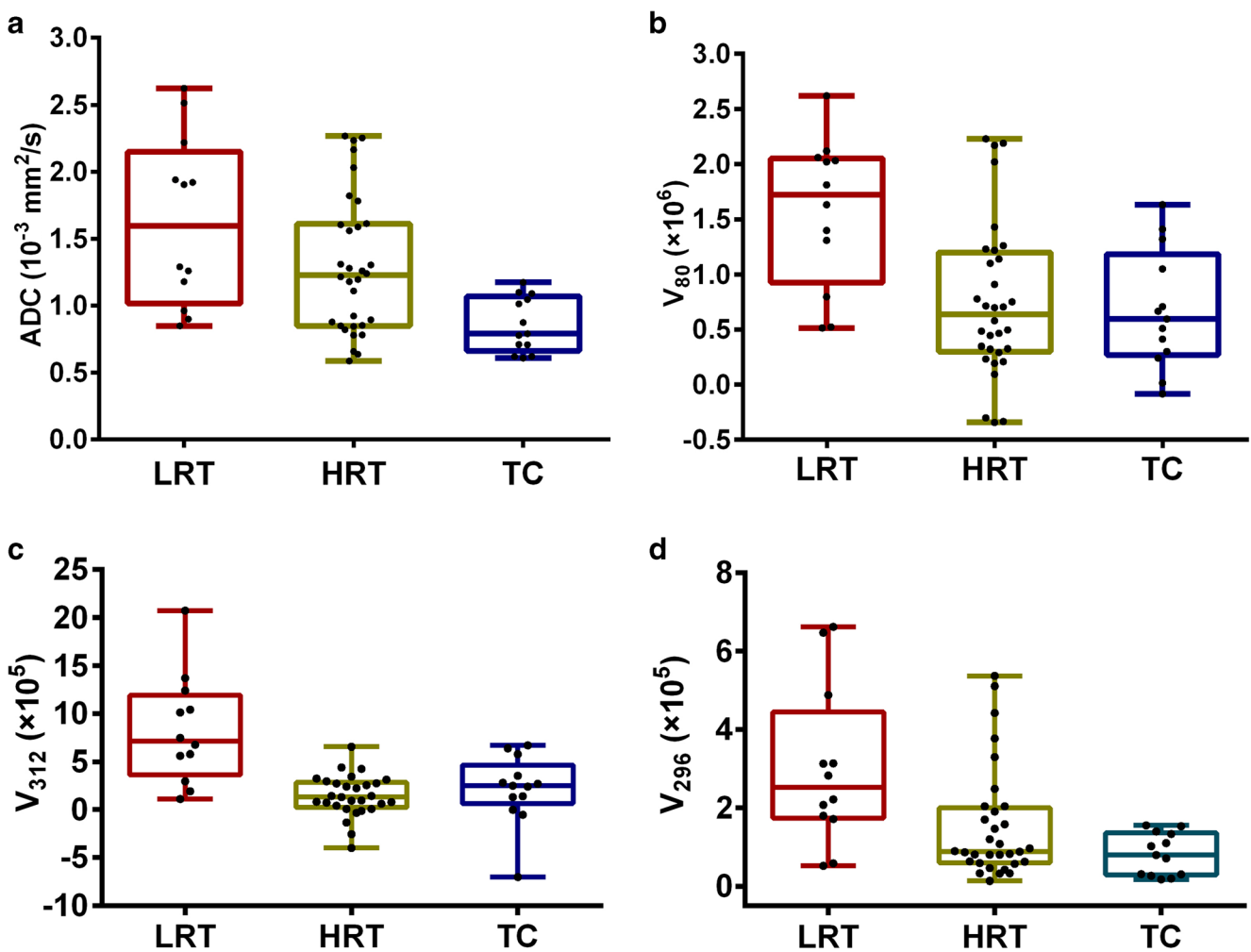


Fig. 3 Box plots for values of ADC (a), V_{80} (b), V_{312} (c), and V_{296} (d) among low-risk thymoma (LRT), high-risk thymoma (HRT), and thymic carcinoma (TC). ADC, apparent diffusion coefficients; V_{80} , Cluster

Shade_angle90_offset1; V_{296} , Cluster Shade_AllDirection_offset6_SD; V_{312} , Cluster Shade_angle45_offset6

Table 4 ADC and DWI texture parameter comparisons between early and advanced stages of thymic epithelial tumors

Parameters	Early stage ($n = 32$)	Advanced stage ($n = 25$)	t	p
ADC ($\times 10^{-3}$ mm ² /s)	1.48 \pm 0.59	1.00 \pm 0.36	3.797	< 0.001
Texture analysis				
V_{57} ($\times 10^7$)	2.56 \pm 2.51	1.39 \pm 0.96	2.408	0.021
V_{204}	9.38 \pm 1.30	10.27 \pm 1.06	2.795	0.007
V_{278} ($\times 10^{-4}$)	1.50 \pm 1.69	2.40 \pm 1.51	2.094	0.041
V_{296} ($\times 10^5$)	2.06 \pm 1.81	1.18 \pm 1.11	2.273	0.027
V_{735} ($\times 10^{-3}$)	5.59 \pm 3.37	3.66 \pm 2.35	2.428	0.018
V_{920}	13.00 \pm 11.29	19.64 \pm 11.49	2.190	0.033
V_{1025}	0.56 \pm 0.06	0.52 \pm 0.07	2.575	0.013
V_{1030}	30.62 \pm 14.42	39.06 \pm 10.02	2.491	0.016
V_{1033}	1.79 \pm 0.19	1.95 \pm 0.26	2.618	0.011

* p values were calculated by the independent samples t test

ADC, apparent diffusion coefficients; V_{57} , Cluster Prominence_AllDirection_offset1_SD; V_{204} , GLCM Entropy_angle0_offset4; V_{278} , Correlation_angle135_offset5; V_{296} , Cluster Shade_AllDirection_offset6_SD; V_{735} , Short Run Emphasis_AllDirection_offset5_SD; V_{920} , High Gray-Level Run Emphasis_AllDirection_offset8_SD; V_{1025} , sphericity; V_{1030} , maximum 3D diameter; V_{1033} , spherical disproportion

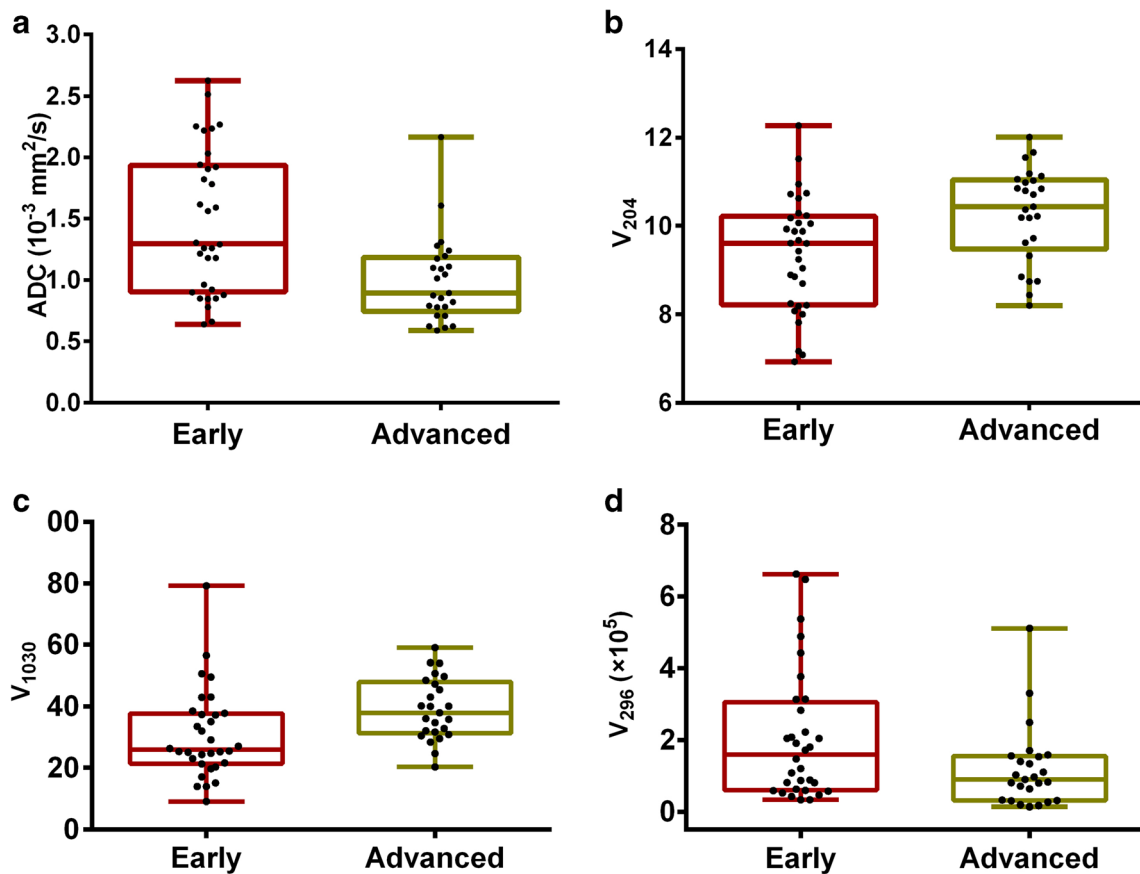


Fig. 4 Box plots for values of ADC (a), V_{204} (b), V_{1030} (c), and V_{296} (d) between early and advanced stages of thymic epithelial tumors. ADC, apparent diffusion coefficients; V_{204} , GLCM Entropy_angle0_offset4; V_{296} , Cluster Shade_AllDirection_offset6_SD; V_{1030} , maximum 3D diameter

showed that several DWI texture parameters were significantly different among various subtypes or stages of TETs. Both V_{80} and V_{312} of cluster shade parameters

measured the skewness and uniformity of the GLCM (gray-level co-occurrence matrix); a higher cluster shade implied greater tumor asymmetry or less homogeneity.

Table 5 Diagnostic efficacy comparisons of ADC and DWI texture parameters in differentiating the defined groups of thymic epithelial tumors (TETs) based on the WHO classification and Masaoka–Koga stage

Parameters	AUC	Sensitivity (%)	Specificity (%)	Cutoff value	<i>p</i>
LRT vs. HRT+TC					
ADC ($\times 10^{-3}$ mm ² /s)	0.746	50.0	90.5	1.86	0.01
V_{80} ($\times 10^6$)	0.862	75.0	88.1	1.29	<0.001
V_{312} ($\times 10^5$)	0.875	75.0	90.5	5.00	<0.001
Logistic (V_{80} , V_{312}) [#]	0.877	90.5	83.3	0.71	<0.001
Logistic (ADC, V_{312}) [#]	0.933	95.2	91.7	0.65	<0.001
Early vs. advanced stage					
ADC ($\times 10^{-3}$ mm ² /s)	0.755	68.8	76.0	1.18	0.001
V_{204}	0.720	68.0	75.0	10.18	0.005
V_{1030}	0.726	92.0	56.3	27.66	0.004
Logistic (ADC, V_{1030}) [#]	0.772	84.0	65.6	0.40	<0.001

**p* values were calculated by the receiver operating characteristic (ROC) curve analyses using SPSS software.

[#] The results of logistic (value 1, value 2) were acquired by using the group as dependent variable and using value 1 and value 2 as covariates to make a binary logistic regression and then acquired each patient's *p* value, and this *p* value will be analyzed by ROC analysis

AUC, area under curve; LRT, low-risk thymoma; HRT, high-risk thymoma; TC, thymic carcinoma; ADC, apparent diffusion coefficients; V_{80} , Cluster Shade_angle90_offset1; V_{204} , GLCM Entropy_angle0_offset4; V_{312} , Cluster Shade_angle45_offset6; V_{1030} , maximum 3D diameter

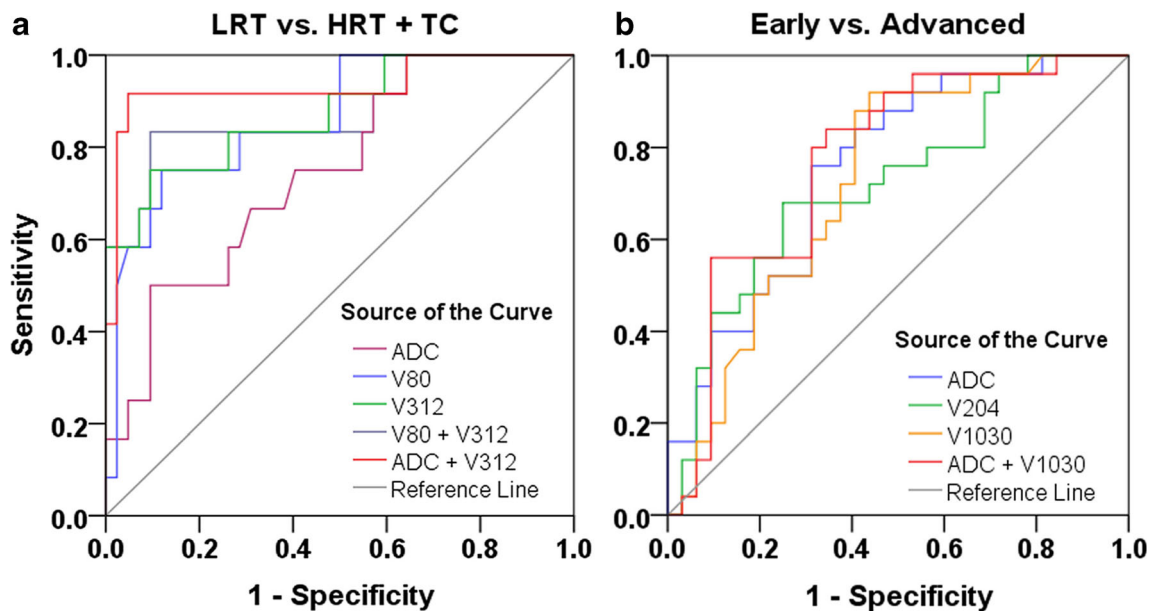


Fig. 5 Receiver operating characteristic curves for the differentiating performance of the ADC and DWI texture parameters among the defined groups of thymic epithelial tumors based on the WHO classification and Masaoka stage. **a** LRT vs. HRT and TC with the ADC, V_{80} and V_{312} value. **b** Early vs. advanced stage with the ADC,

V_{204} and V_{1030} value. LRT, low-risk thymoma; HRT, high-risk thymoma; TC, thymic carcinoma; ADC, apparent diffusion coefficient; V_{80} , Cluster Shade_angle90_offset1; V_{312} , Cluster Shade_angle45_offset6; V_{204} , GLCM Entropy_angle0_offset4; V_{1030} , maximum 3D diameter

Interestingly, according to our results, V_{80} and V_{312} values were significantly higher in LRT than those in HRT or TC, indicating lower tumor homogeneity in LRT, which was out of our expectation. In most cases, malignant tumors have higher tumor heterogeneity due to more necrotic and heterogeneous growth than benign or low-grade malignancies. However, macroscopic appearance of multiple nodules separated by fibrous bands was demonstrated in LRT especially in over 77% of type AB thymomas, and the typical growth pattern is less in HRT and none in TC [11], which might explain why the significant higher V_{80} and V_{312} values exist in LRT. In addition, V_{1030} (maximum 3D diameter) values were significantly lower in LRT than those in HRT or TC in the current study, which were consistent with previous results of longer diameter in advanced stages of TETs than in LRT or early stages [19].

Furthermore, we evaluated the diagnostic efficacy of ADC values and DWI texture parameters in differentiating the TET types and stages. The results showed that V_{80} and V_{312} achieve relatively good performance, and the binary logistic regression analysis with combination of ADC and V_{312} revealed the highest efficacy, with an AUC of 0.933, in differentiating the LRT from the HRT or TC. Interestingly, the combination of two texture parameters did not improve the differentiating efficacy, and the reason for such a result could be that V_{80} and V_{312} belong to a category of cluster shade feature. Chiefly, combining ADC and V_{312} could potentially be useful as a predicting biomarker of TET subtypes.

As in the previous studies with various imaging modalities [9, 14, 19, 20], in this study, both the ADC value and DWI texture parameters did not obtain excellent differentiating ability for different stages of TETs. Indeed, there was no unequivocal correlation between pathological subtypes and stages [19]; all of the types of TETs can follow an aggressive clinical course [2], which might explain in part relatively low performance in predicting the stages of TETs [9].

In addition, significant differences were found in form factor parameters of V_{1025} , V_{1030} , and V_{1033} between early- and advanced-stage TETs. These features describe the three-dimensional size and shape of the tumor region, mainly decided by the volume and the surface area of the VOI according to the formula. In this study, the VOI was maintained at a distance of 1–2 mm away from the tumor margin to avoid the effects of edge noise and partial volume phenomenon [37], which could potentially affect the volume and surface area of the VOI and therefore affect the form factor parameters. Although segmentation is of critical importance, as there is no defined ground truth, reproducibility of segmentation becomes an important issue [38]. Therefore, further research may be warranted to clarify this problem.

There are several limitations of this study. Firstly, although this was the largest series of TETs evaluated with DWI, the sample size was relatively small, mainly because of the low clinical incidence of thymic tumors. Secondly, we calculated the ADC value by drawing ROIs of focal tumor areas by one reader. Further histogram analysis based on the whole tumor

and the calculation of inter-class correlation coefficient might be needed to reduce sampling bias and assess inter-observer repeatability of the measurements. In addition, we used the b_0 image and b_{1000} image to obtain the ADC values in the monoexponential model of DWI, which could be overestimated due to the perfusion bias, and the use of perfusion-free ADC measurements by minimum b value of 100–150 s/mm² instead of 0 s/mm² might avoid this problem properly [39, 40]. Thirdly, ten advanced-stage TET patients did not undergo surgery owing to the widespread invasion or metastasis, which was proved by puncture biopsy and staged by imaging, and thereby might cause a study bias. Finally, as a preliminary study to explore the possibility of using DWI texture analysis for obtaining quantitative biomarkers of TETs, further radiomics study with bigger samples is needed to clarify this issue.

In conclusion, several parameters derived from DWI texture analysis could be useful in distinguishing pathological subtypes or stages of TETs, and combination of ADC and texture indices improved the differentiating diagnosis efficacy.

Acknowledgements We would like to thank Dr. Xiao-Cheng Wei in GE Healthcare China for providing technical support regarding the application of Analysis-Kit software and supplementary Material (Texture Parameters Description.PDF).

Funding This study has received funding from the Science and Technology Innovation Development Foundation of Tangdu Hospital (no. 2017LCYJ004).

Compliance with ethical standards

Guarantor The scientific guarantor of this publication is Guang-bin Cui.

Conflict of interest The authors of this manuscript declare no relationships with any companies, whose products or services may be related to the subject matter of the article.

Statistics and biometry Lei Shang kindly provided statistical advice for this manuscript.

Informed consent Written informed consent was waived by the Institutional Review Board.

Ethical approval Institutional Review Board approval was obtained.

Study subjects or cohorts overlap Some study subjects or cohorts have been previously reported in Li GF, Duan SJ, Yan LF, et al Intravoxel incoherent motion diffusion-weighted MR imaging parameters predict pathological classification in thymic epithelial tumors. *Oncotarget* 2017;8(27):44579–44592.

Methodology

- retrospective
- diagnostic or prognostic study
- performed at one institution

References

- Engels EA (2010) Epidemiology of thymoma and associated malignancies. *J Thorac Oncol* 5:S260–S265
- Weis CA, Yao X, Deng Y et al (2015) The impact of thymoma histotype on prognosis in a worldwide database. *J Thorac Oncol* 10:367–372
- Masaoka A, Monden Y, Nakahara K, Tanioka T (1981) Follow-up study of thymomas with special reference to their clinical stages. *Cancer* 48:2485–2492
- Moon JW, Lee KS, Shin MH et al (2015) Thymic epithelial tumors: prognostic determinants among clinical, histopathologic, and computed tomography findings. *Ann Thorac Surg* 99:462–470
- Ried M, Marx A, Gotz A, Hamer O, Schalke B, Hofmann HS (2016) State of the art: diagnostic tools and innovative therapies for treatment of advanced thymoma and thymic carcinoma. *Eur J Cardiothorac Surg* 49:1545–1552
- Padda SK, Terrone D, Tian L et al (2018) Computed tomography features associated with the eighth edition TNM stage classification for thymic epithelial tumors. *J Thorac Imaging* 33:176–183
- Huang J, Detterbeck FC, Wang Z, Loehrer PJ Sr (2010) Standard outcome measures for thymic malignancies. *J Thorac Oncol* 5: 2017–2023
- Falkson CB, Bezjak A, Darling G et al (2009) The management of thymoma: a systematic review and practice guideline. *J Thorac Oncol* 4:911–919
- Li GF, Duan SJ, Yan LF et al (2017) Intravoxel incoherent motion diffusion-weighted MR imaging parameters predict pathological classification in thymic epithelial tumors. *Oncotarget* 8:44579–44592
- Marom EM (2013) Advances in thymoma imaging. *J Thorac Imaging* 28:69–80
- Hu YC, Wu L, Yan LF et al (2014) Predicting subtypes of thymic epithelial tumors using CT: new perspective based on a comprehensive analysis of 216 patients. *Sci Rep* 4:6984
- Ozawa Y, Hara M, Shimohira M, Sakurai K, Nakagawa M, Shibamoto Y (2016) Associations between computed tomography features of thymomas and their pathological classification. *Acta Radiol* 57:1318–1325
- Sadohara J, Fujimoto K, Muller NL et al (2006) Thymic epithelial tumors: comparison of CT and MR imaging findings of low-risk thymomas, high-risk thymomas, and thymic carcinomas. *Eur J Radiol* 60:70–79
- Jing Y, Yan WQ, Li GF et al (2018) Usefulness of volume perfusion computed tomography in differentiating histologic subtypes of thymic epithelial tumors. *J Comput Assist Tomogr* 42:594–600
- Henzler T, Schmid-Bindert G, Schoenberg SO, Fink C (2010) Diffusion and perfusion MRI of the lung and mediastinum. *Eur J Radiol* 76:329–336
- Priola AM, Gned D, Veltri A, Priola SM (2016) Chemical shift and diffusion-weighted magnetic resonance imaging of the anterior mediastinum in oncology: current clinical applications in qualitative and quantitative assessment. *Crit Rev Oncol Hematol* 98:335–357
- Coolen J, De Keyzer F, Nafteux P et al (2012) Malignant pleural disease: diagnosis by using diffusion-weighted and dynamic contrast-enhanced MR imaging—initial experience. *Radiology* 263:884–892
- Razek AA (2012) Diffusion magnetic resonance imaging of chest tumors. *Cancer Imaging* 12:452–463
- Abdel Razek AA, Khairy M, Nada N (2014) Diffusion-weighted MR imaging in thymic epithelial tumors: correlation with World Health Organization classification and clinical staging. *Radiology* 273:268–275

20. Priola AM, Priola SM, Giraudo MT et al (2015) Diffusion-weighted magnetic resonance imaging of thymoma: ability of the apparent diffusion coefficient in predicting the World Health Organization (WHO) classification and the Masaoka-Koga staging system and its prognostic significance on disease-free survival. *Eur Radiol* 26: 2126–2138
21. Asselin MC, O'Connor JP, Boellaard R, Thacker NA, Jackson A (2012) Quantifying heterogeneity in human tumours using MRI and PET. *Eur J Cancer* 48:447–455
22. Choi MH, Lee YJ, Yoon SB, Choi JI, Jung SE, Rha SE (2018) MRI of pancreatic ductal adenocarcinoma: texture analysis of T2-weighted images for predicting long-term outcome. *Abdom Radiol (NY)*. <https://doi.org/10.1007/s00261-018-1681-2>
23. Tian Q, Yan LF, Zhang X et al (2018) Radiomics strategy for glioma grading using texture features from multiparametric MRI. *J Magn Reson Imaging* 48:1518–1528
24. Skogen K, Schulz A, Helseth E, Ganeshan B, Dormagen JB, Server A (2018) Texture analysis on diffusion tensor imaging: discriminating glioblastoma from single brain metastasis. *Acta Radiol*. <https://doi.org/10.1177/0284185118780889>
25. Fritz B, Muller DA, Sutter R et al (2018) Magnetic resonance imaging-based grading of cartilaginous bone tumors: added value of quantitative texture analysis. *Invest Radiol* 53:663–672
26. Jiang X, Xie F, Liu L, Peng Y, Cai H, Li L (2018) Discrimination of malignant and benign breast masses using automatic segmentation and features extracted from dynamic contrast-enhanced and diffusion-weighted MRI. *Oncol Lett* 16:1521–1528
27. Nakajo M, Jinguji M, Shinaji T et al (2018) Texture analysis of (18)F-FDG PET/CT for grading thymic epithelial tumours: usefulness of combining SUV and texture parameters. *Br J Radiol* 91:20170546
28. Luciani A, Vignaud A, Cavet M et al (2008) Liver cirrhosis: intravoxel incoherent motion MR imaging—pilot study. *Radiology* 249:891–899
29. Li Z, Zhang D, Dai Y et al (2018) Computed tomography-based radiomics for prediction of neoadjuvant chemotherapy outcomes in locally advanced gastric cancer: a pilot study. *Chin J Cancer Res* 30: 406–414
30. Travis WDBE, Müller-Hermelink HK, Harris CC (2004) World Health Organization classification of tumours. Pathology and genetics of tumours of the lung, thymus and heart. IARC Press, Lyon, pp 152–153
31. Jeong YJ, Lee KS, Kim J, Shim YM, Han J, Kwon OJ (2004) Does CT of thymic epithelial tumors enable us to differentiate histologic subtypes and predict prognosis? *AJR Am J Roentgenol* 183:283–289
32. Hoang UN, Mojdeh Mirmomen S, Meirelles O et al (2018) Assessment of multiphase contrast-enhanced MR textures in differentiating small renal mass subtypes. *Abdom Radiol (NY)* 43: 3400–3409
33. Lee HS, Jang HJ, Shah R et al (2017) Genomic analysis of thymic epithelial tumors identifies novel subtypes associated with distinct clinical features. *Clin Cancer Res* 23:4855–4864
34. Girard N, Ruffini E, Marx A, Faivre-Finn C, Peters S, Committee EG (2015) Thymic epithelial tumours: ESMO clinical practice guidelines for diagnosis, treatment and follow-up. *Ann Oncol* 26(Suppl 5):v40–v55
35. Lee HS, Oh JS, Park YS, Jang SJ, Choi IS, Ryu JS (2016) Differentiating the grades of thymic epithelial tumor malignancy using textural features of intratumoral heterogeneity via (18)F-FDG PET/CT. *Ann Nucl Med* 30:309–319
36. Ganeshan B, Goh V, Mandeville HC, Ng QS, Hoskin PJ, Miles KA (2013) Non-small cell lung cancer: histopathologic correlates for texture parameters at CT. *Radiology* 266:326–336
37. Feng Z, Rong P, Cao P et al (2018) Machine learning-based quantitative texture analysis of CT images of small renal masses: differentiation of angiomyolipoma without visible fat from renal cell carcinoma. *Eur Radiol* 28:1625–1633
38. Park JE, Kim HS (2018) Radiomics as a quantitative imaging biomarker: practical considerations and the current standpoint in neuro-oncologic studies. *Nucl Med Mol Imaging* 52:99–108
39. Padhani AR, Liu G, Koh DM et al (2009) Diffusion-weighted magnetic resonance imaging as a cancer biomarker: consensus and recommendations. *Neoplasia* 11:102–125
40. Priola AM, Priola SM, Gned D et al (2016) Diffusion-weighted quantitative MRI to diagnose benign conditions from malignancies of the anterior mediastinum: improvement of diagnostic accuracy by comparing perfusion-free to perfusion-sensitive measurements of the apparent diffusion coefficient. *J Magn Reson Imaging* 44: 758–769

Publisher's note Springer Nature remains neutral with regard to jurisdictional claims in published maps and institutional affiliations.